SI Appendix

Mitotic and pheromone-specific intrinsic polarization cues interfere with gradient sensing in *S. cerevisiae*

Gustavo Vasen[1,2], Paula Dunayevich[1,2] and Alejandro Colman-Lerner[1,2]*

[1] Department of Physiology, Molecular and Cellular Biology, School of Exact and Natural Sciences, University of Buenos Aires, Buenos Aires, Argentina

[2] Institute of Physiology, Molecular Biology and Neurosciences, National Scientific and Technical Research Council (IFIBYNE-CONICET), Buenos Aires, Argentina

*Corresponding author. Tel: +54 11 4576 3368; E-mail: colman-lerner@fbmc.fcen.uba.ar

Table of contents

www.pnas.org/cgi/doi/10.1073/pnas.1912505117

Supplementary Figures

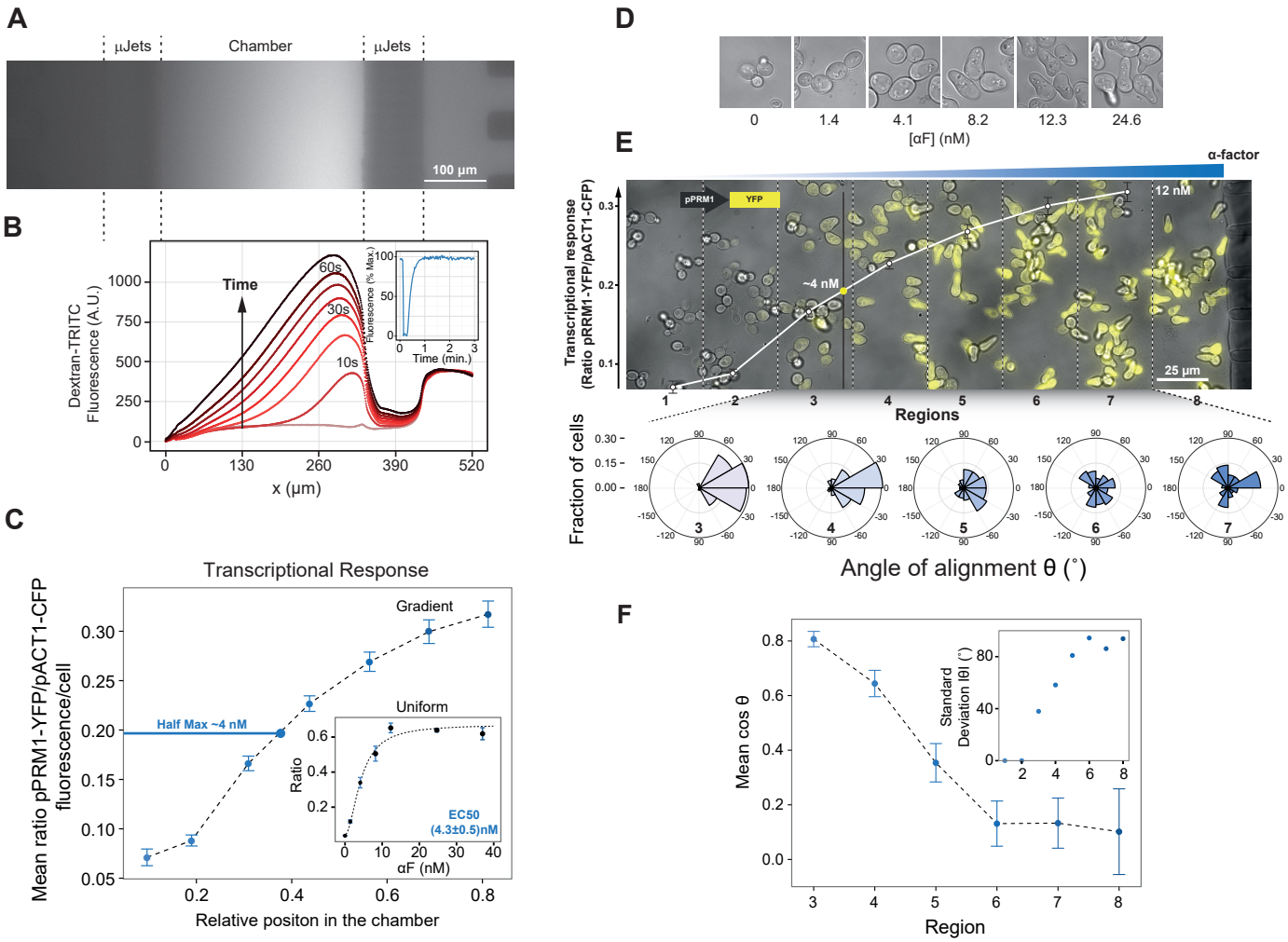

Figure S1. Microfluidic device, related to Figure 2.

A. Open chamber microfluidic device (1). The 300-µm chamber is flanked by microjets (µJets), from which medium (left) or medium containing α-factor in combination with TRITC-Dextran (right) diffuses out. Image was taken using 20X magnification and the Texas Red filter cube. **B.** A linear gradient is quickly formed on the surface. Plot shows TRITC fluorescence vs x position measured at the indicated times after washing with medium. Plot is aligned with the chamber shown in A. **Inset**. Dynamics of gradient formation. Plot shows the average fluorescence (relative to the signal before the wash) vs. time of a square of 100-µm side centered at position 150 µm in the x-axis. **C.** Calibration of actual concentration of α-factor in the gradient. *Δbar1* cells (TCY3154) that express the α-factor inducible P_{PRM1}-*YFP* and P_{ACT1}-*CFP* reporters were exposed to a linear pheromone gradient (or the indicated uniform concentrations, **Inset**) for 2 h. The ratio of YFP/CFP was used to correct for differences in expression capacity (2). **Inset.** With uniform stimulation, the transcriptional response saturated at 12nM with an EC50 of 4 nM, based on a Hill equation fit (dashed lined). For the gradient conditions, the chamber from our devices was divided in eight regions. The YFP/CFP ratio saturates usually in the rightmost 50-µm region (closest to the α-factor source). Therefore, we considered the concentration of α-factor in this region to be around 12 nM. Based on this, the half-maximal response corresponds to the expected EC50 of around 4 nM, between regions 3 and 4. **D.** Morphology of yeast stimulated with the indicated uniform α-factor concentrations. **E.** Representative image of TCY3154 cells in the microfluidic device after 3 h. YFP fluorescence is displayed in yellow. The transcriptional response (ratio YFP/CFP) from **C** is overlaid on the image to indicate the local α-factor concentration. Note that the morphology at each region matches the morphology of yeast exposed to uniform concentrations of α-factor (**D**). **Bottom**. In each region, the angle of alignment between the mating projection (MP) and the gradient, θ, was calculated. Polar plots show the distribution of θ in sectors 3 through 7. **F.** Gradient-sensing performance was assessed as the mean of cosine θ in each region together with the standard deviation of θ (inset).

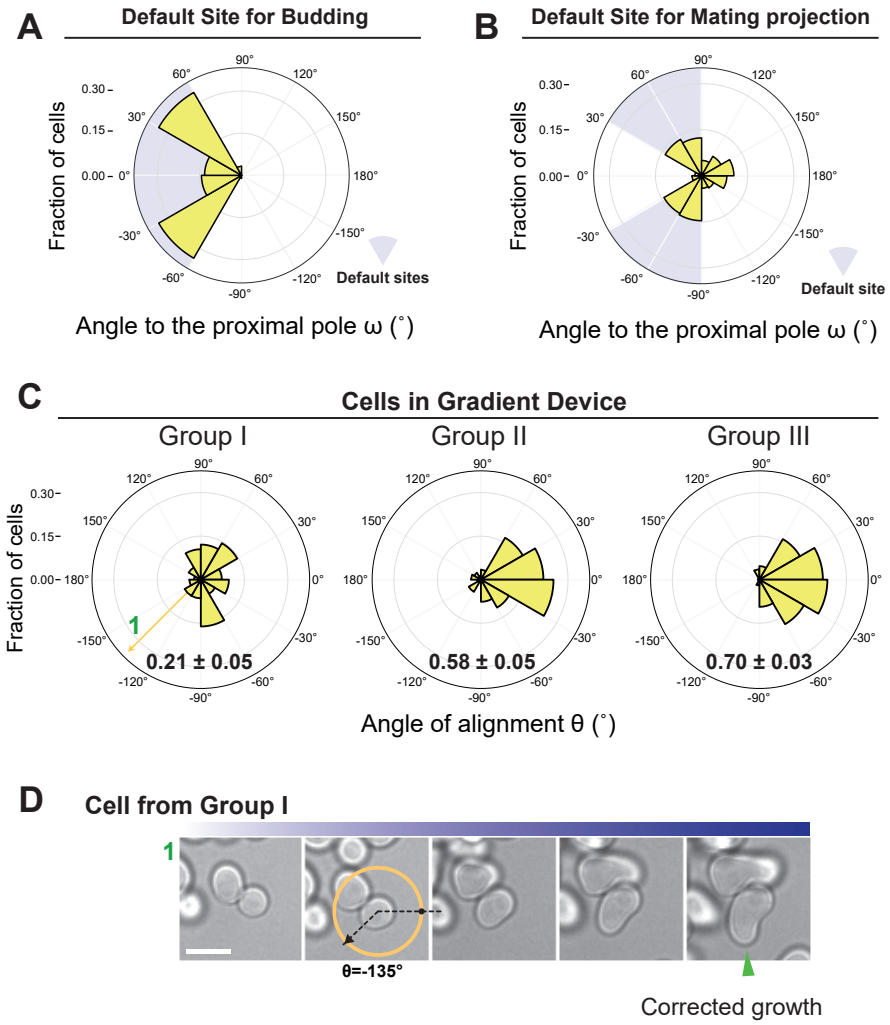

Figure S2. Internal polarity cues interfere with gradient sensing in cells of the S288C genetic background, related to Figure 2.

A-B. Budding (**A**) and MP (**B**) default sites used by a MATa *Δbar1* S288C-derivative strain (YDV5654). Yeast were imaged during vegetative growth or after stimulation with uniform (no gradient) 5-nM αF. In daughter cells, the angle between the proximal pole and the first bud or MP, ω, was measured as illustrated by the diagram in Figure 1C. Polar plots show distributions of ω. Cells used the region next to the proximal pole both for budding and MP formation. Note the "no-polarization zone" at angles between -30º and 30º. **C.** YDV5654 cells were exposed to a gradient of α-factor in a microfluidic device. Daughter cells were divided into three groups depending on ϕ (Figure 1C): I, distal pole facing the gradient ($|\phi| > 120º$); II, distal pole perpendicular to the gradient ($60º < |\phi| < 120º$); III, distal pole facing away from the gradient ($|\phi| < 60º$). Polar plots show the distributions of θ, the angle of alignment, where 0° corresponds to perfect alignment. The mean cosθ ± SEM is indicated in each group. Note the poor alignment by cells in Group I. The arrow indicates the angle of alignment of the example cell shown in **D**. The data from two independent experiments were pooled (total number of cells: 460). **D**. Example of a cell from Group I. θ is indicated. The pheromone source is on the right. Scale bar: 5 μm.

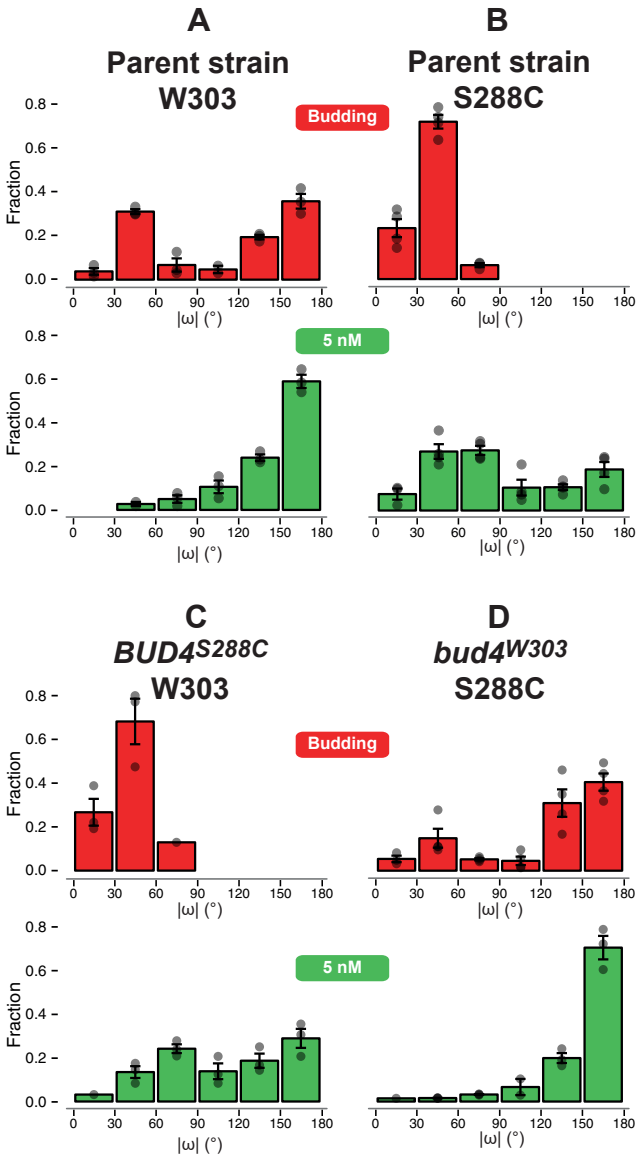

Figure S3. Default budding site and MP positioning in *BUD4* and *bud4* strains, related to Figure 2.

Distribution of angles ω in daughter cells for the first bud (red) or the MP in response to uniform 5-nM α-factor (green) in the parent strains derived from (**A**) W303 (ACL379) or (**B**) S288C (YDV5654), or in the strains in which we swapped *BUD4* alleles: (**C**) W303 *Δbar1 BUD4*^{S288C} (YGV5765) and (**D**) S288C *Δbar1 bud4*^{W303} (YGV5831). In all cases, angle distributions were divided in 30° bins and the fractions of cells in each bin were calculated. Note that the data for strains ACL379 and YDV5654 are the same as in Figure 2A-B and S2A-B, but displayed in a linear histogram (absolute value of ω). Data from at least three-four independent experiments were pooled to calculate the means ± SEMs (bars and whiskers).

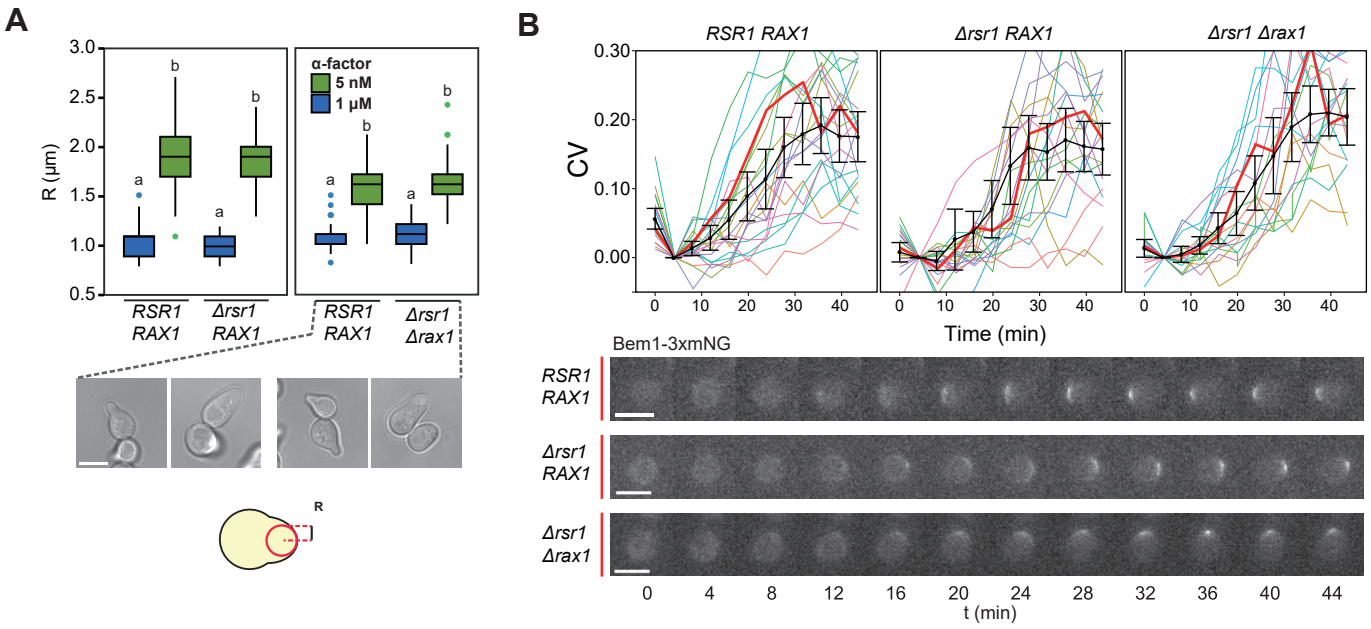

Figure S4. Mating projection shape and polarization dynamics in *Δrsr1* and *Δrsr1Δrax1* strains, related to Figure 3.

A. MP size was estimated as the radius of a circumference that fits in the projection (diagram). Boxplots show the radii from independent experiments done with yeast of the indicated genotypes, exposed for 2 h to high (1 μM, blue) or low (5 nM, green) α-factor. *RAX1 RSR1* is the W303 *Δbar1* strain ACL379. *Δrsr1 RAX1* (YGV5405) and *Δrsr1Δrax1* (YGV5838) are derivatives of ACL379. Statistical comparisons were calculated by two-way ANOVA followed by Tukey post-test: left, a vs b, $p<0.001$; right, a vs b, $p<0.001$. Images illustrate yeast of the indicated genotypes. **B.** Polarization dynamics were measured as the increases in the coefficient of variation (CV) of the distribution of Bem1-mNG in each cell, a method based on (3). Plot shows examples of individual cells (color traces) and the means of the populations (black) ± SEM, as a function of time after addition of 1-μM α-factor, for the indicated strains. Time-lapse shows one example of each *RAX1 RSR1*, *Δrsr1 RAX1*, and *Δrax1Δrsr1* cells (thicker red lines in the plots). Bars corresponds to 5 μm. Strains are derivatives from strains in **A**: *RAX1 RSR1 BEM1-3xmNG* (YGV5097), *Δrsr1 RAX1 BEM1-3xmNG* (YGV5486), and *Δrax1Δrsr1 BEM1-3xmNG* (YGV5879).

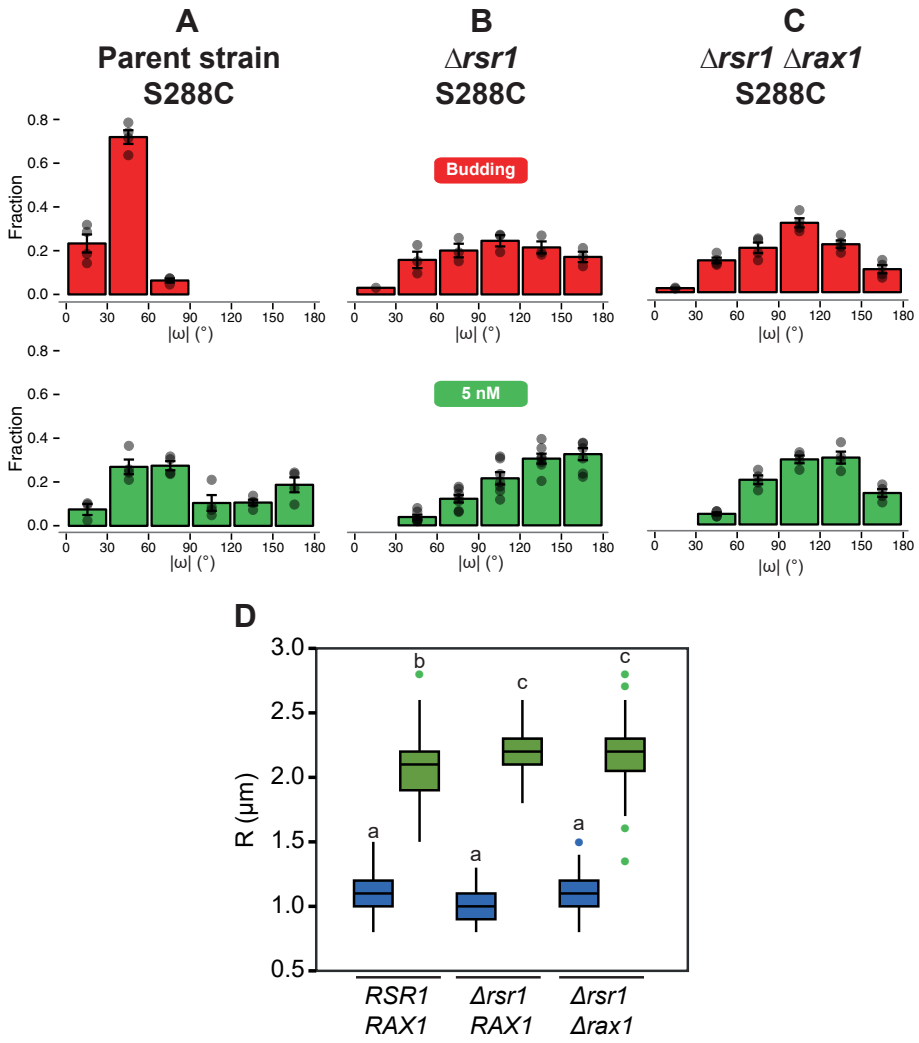

Figure S5. Default budding site and MP positioning in *Δrsr1* and *Δrsr1Δrax1* S288C-derivatives, related to Figure 3.

A-C. Distribution of angles ω in daughter cells for the first bud (red) or the MP in response to uniform 5-nM α-factor (green) in the *Δbar1* parent strain (**A**) and *Δrsr1* (**B**) and *Δrax1Δrsr1* (**C**) derivatives in the S288C genetic background. In all cases, angle distributions were divided in 30° bins and the fraction of cells in each bin was calculated. Data from at least three-four independent experiments were pooled to calculate the means ± SEMs (bars and whiskers). Strains: S288C *Δbar1* parent strain (YDV5654); S288C *Δrsr1* (YGV5655), and S288C *Δrsr1 Δrax1* (YDV6164). **D.** MP size was estimated as the radius of a circumference that fits in the projection in cells from **A-B**. Boxplots show the radius from independent experiments done with yeast of the indicated genotypes, exposed for 2 h to high (1 µM, blue) or low (5 nM, green) α-factor. Statistical comparisons were calculated by two-way ANOVA follow by Tukey post-test: a vs. b, c, $p<0.001$; b vs. c, $p<0.03$. Note the subtle increase in MP width observed in *Δrsr1* derivatives as previously reported (4). This difference was not observed in the W303 genetic background (Figure S4).

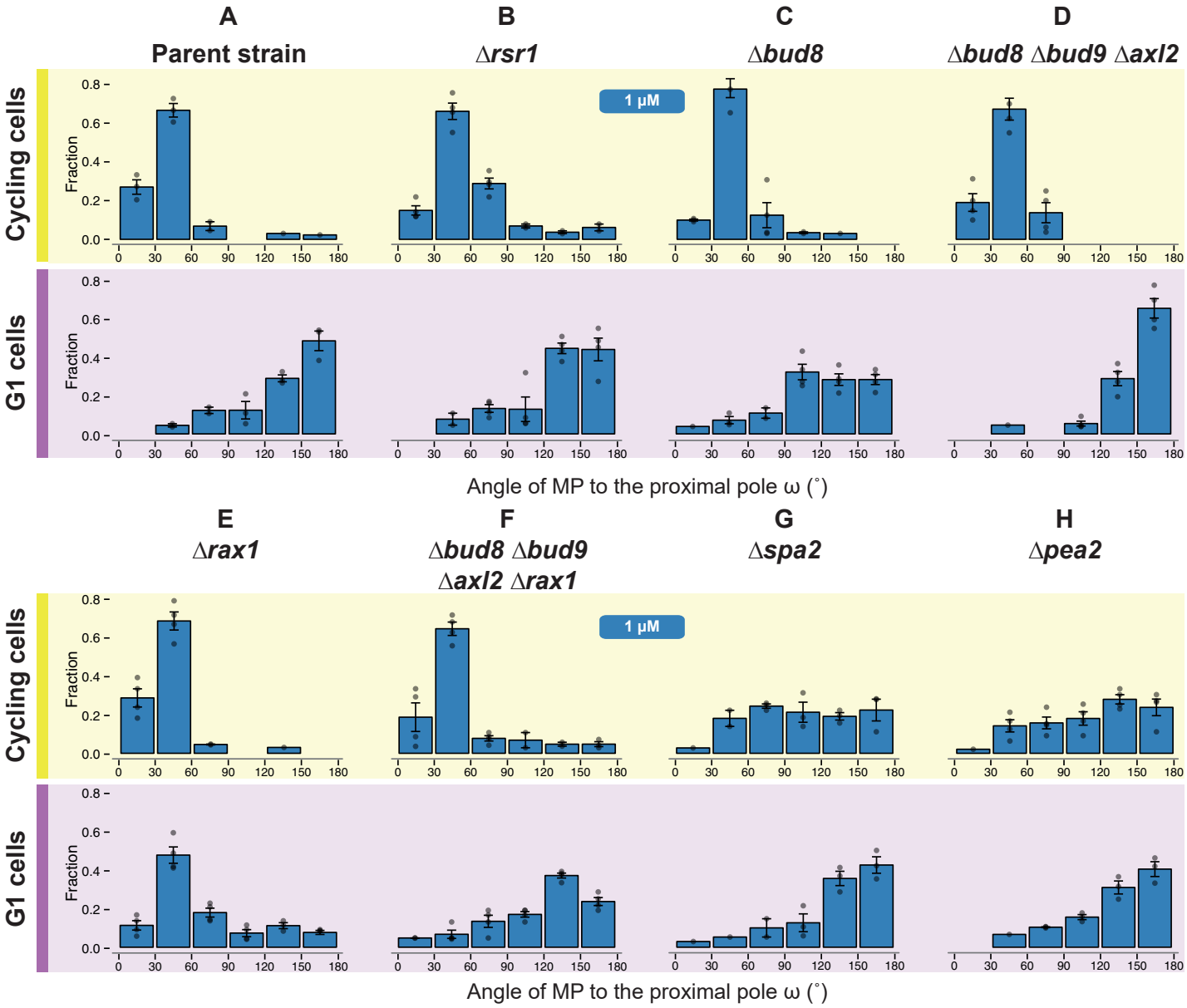

Figure S6. Default MP positioning at high α-factor concentration depends on cell-cycle position at the time of pheromone stimulation, related to Figure 4.

Distributions of angles ω in daughter cells exposed to 1-µM α-factor for 2 h. Cells were classified depending on cell-cycle position as "cycling cells" if they were buds at the moment of pheromone exposure or "G1 cells" if they were already in G1. In all cases, angle distributions were divided in 30° bins, and the fraction of cells in each bin was calculated. Data from at least three independent experiments (circles), for the indicated strains: W303 parent strain (ACL379); *Δrsr1* (YGV5405); *Δbud8* (YGV5429); *Δbud8 Δbud9 Δaxl2* (YGV5433); *Δrax1* (YGV5259); *Δbud8 Δbud9 Δaxl2 Δrax1* (YGV5839); *Δspa2* (YRB3862); *Δpea2* (YRB3865).

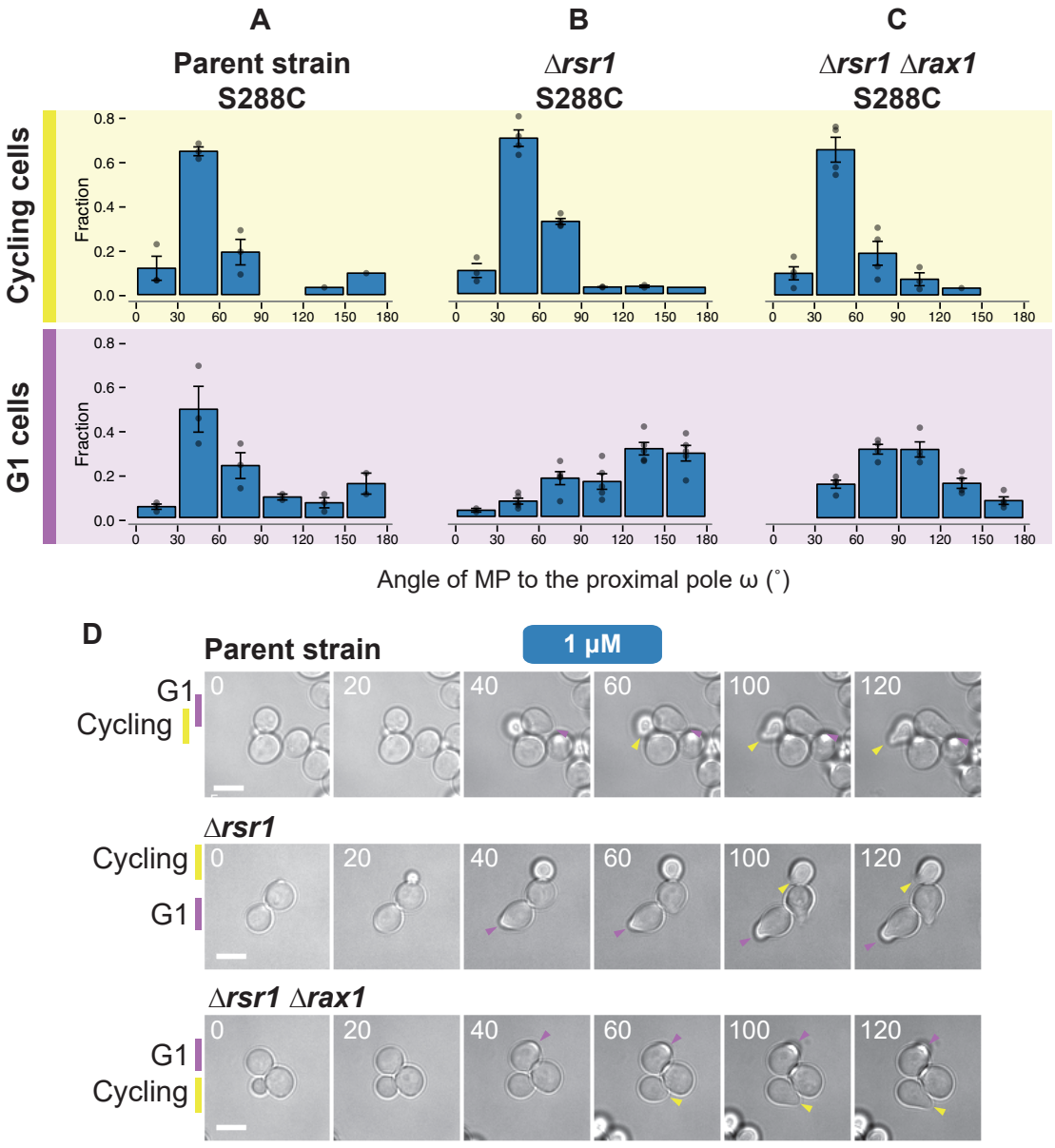

Figure S7. Default MP positioning at high α-factor concentration in S288C-derived cells depends on cell-cycle position at the time of pheromone stimulation, related to Figure 4.

A-C. Distributions of angles ω in daughter cells exposed to 1-μM α-factor for 2 h. Cells were classified depending on cell-cycle position as "cycling cells" if they were buds at the moment of pheromone exposure or "G1 cells" if they were already in G1. In all cases, angle distributions were divided in 30° bins, and the fraction of cells in each bin was calculated. Data from at least three independent experiments (circles), for the indicated strains: S288C parent strain (YDV5654); S288C *Δrsr1* (YGV5655), and S288C *Δrsr1 Δrax1* (YDV6164). **D**. Time-lapse images of cells from **A-C** stimulated with 1-μM α-factor. Arrowheads indicate the position of the mating projection for G1 (violet) and cycling (yellow) cells. Numbers correspond to time in minutes. Scale bar: 5 μm.

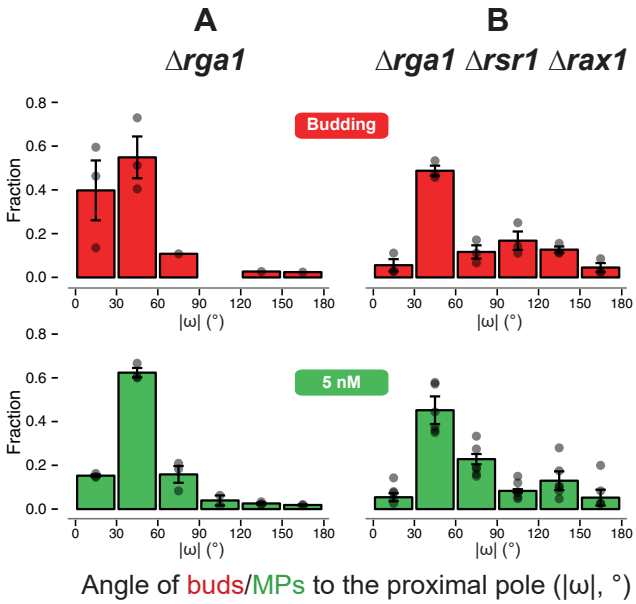

Figure S8. Default MP positioning at low α-factor concentration in cycling cells lacking the Cdc42 inhibitor Rga1, related to Figure 6.

Distributions of angles ω in daughter cells for first buds (red) or MPs in response to uniform 5-nM α-factor (green) in cycling W303-background *Δrga1* (**A**) and *Δrga1 Δrsr1 Δrax1* (**B**) cells. In all cases, angle distributions were divided in 30° bins, and the fraction of cells in each bin was calculated. Data are from at least three independent experiments (circles). Strains: *Δrga1* (YGV6017); *Δrga1 Δrsr1 Δrax1* (YGV6035).

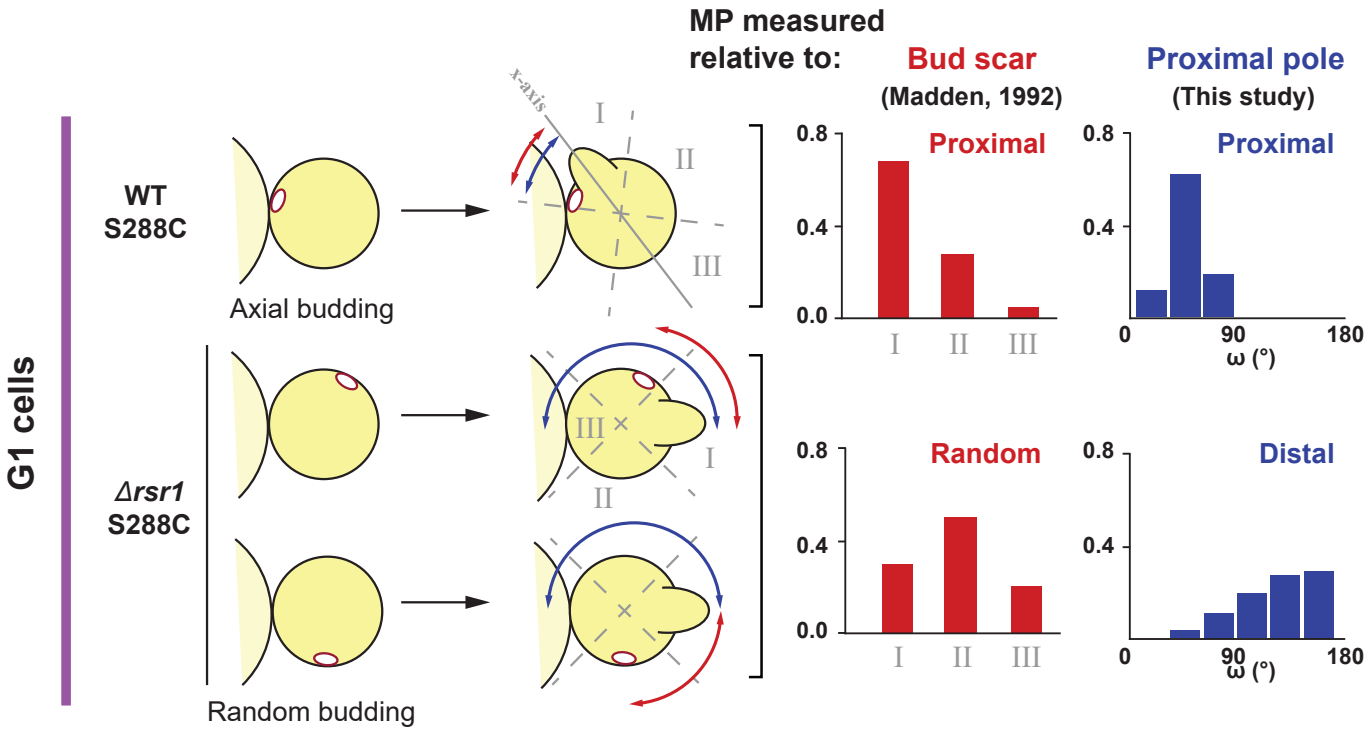

Figure S9. Re-interpretation of original data from Madden and Snyder (1992).

In the original work (main text ref. 38), MP positioning was scored on cells with only one bud scar as revealed by Calcofluor White staining. In these diagrams, we show these cells next to their mothers to highlight the position of the proximal pole/birth scar. Madden and Snyder quantified the distribution of sites selected for mating-projection formation by dividing each cell into three distinct domains. These domains were determined relative to an x-axis running the length of the cell specified by the projection. Class I cells contained the bud scar located -45 to +45° from the x-axis at the end of the cell containing the projection. Class III cells contained the bud scar -45 to +45°from the horizontal axis on the other side of the cell. Class II cells contained the bud scar in the middle region. The boundaries between classes are indicated by dashed lines. Since in wild-type S288C cells (the strain used by the authors), the budding pattern is axial, the previous daughter (and bud scar) would be also at the proximal pole, and thus class I category is the most populated. However, in *Δrsr1* cells, the scenario is different. Based on our data, MPs are formed at the distal pole (180° relative to the proximal pole, blue line) in a Rax1-dependent way. Under our scoring, these would be distal-pole MPs. But, in the earlier analysis, the previous bud scar was used as reference. Given the random-budding phenotype, this reference is located randomly relative to the proximal pole. So, the seemingly random MP site selection in the cells was merely a consequence of the random budding and not of random positioning of the MPs. The misinterpretation of the data explains why distal-pole MP site selection in *Δrsr1* went unnoticed. In the plots on the right we compared the results reported by Madden and Snyder (red) with ours (taken from Figure S5B).

Supplementary Movies

Supplementary Movie 1.

Time-lapse fluorescence microscopy of an example G1 wild-type cell expressing Bem1 fused to three copies of the mNeonGreen fluorescent protein (Bem1-3xmNG, YGV5097) exposed to 1 μM α-factor. Time between frames is ~8 min; last frame, 158 min. Related to Figure 5B.

Supplementary Movie 2.

Time-lapse fluorescence microscopy of an example wild-type cycling cell expressing Bem1 fused to three copies of the mNeonGreen fluorescent protein (Bem1-3xmNG, YGV5097) exposed to 1 μM α-factor. Time between frames is ~8 min; last frame, 109 min. Related to Figure 5B.

Supplementary Movie 3.

Time-lapse fluorescence microscopy of N-terminally YFP-tagged Ste4 (YFP-Ste4, TCY3064) in vegetatively growing cells. Time between frames is ~16 min; last frame 160 min. Related to Figure 5C.

Supplementary Movie 4.

Time-lapse fluorescence microscopy of N-terminally-YFP tagged Ste4 (YFP-Ste4, TCY3064) in cycling cells exposed to 1 μM α-factor. Time between frames is ~16 min; last frame, 208 min. Related to Figure 5C.

Supplementary Movie 5.

Time-lapse fluorescence microscopy of an example wild-type cycling cell expressing Bem1 fused to three copies of the mNeonGreen fluorescent protein (Bem1-3xmNG, YGV5097) exposed to 5 nM α-factor. Time between frames is ~8 min; last frame, 122 min. Related to Figure 6A.

Supplementary Movie 6.

Time-lapse fluorescence microscopy of an example *Δspa2* cycling cell expressing Bem1 fused to three mNeonGreen fluorescent proteins (Bem1-3xmNG, YGV5836) exposed to 5 nM α-factor. Time between frames is ~8 min; last frame, 114 min. Related to Figure 6C.

Supplementary Methods

Yeast strains

Yeast strains used in this study are listed in Table S2. Standard yeast molecular and genetic procedures were used to generate the strains. All strains were generated either from ACL379 (2) or YDV5654, which are *Δbar1* derivatives of W303-1A and BY4741, respectively.

All deletion strains were constructed by the one-step PCR-mediated method using plasmids pFA6a-HIS3MX6, pFA6a-KANMX6, pFA6a-TRP1, pFA6a-NATMX6, or pFA6a-HphNT2 as templates (6). In all cases, forward primers included 40 nucleotide homology arms (-40 to -1 from the ATG) and the F1 sequence, and reverse primers contained 40 nucleotide sequences following the stop codon plus the R1 primer sequence. Screening was performed by PCR and, when possible, by analyzing the budding pattern by live-cell microscopy.

For tagging endogenous Bem1, a PCR-based method was also used with the plasmid pFA6a-3xmNeonGreen-HIS3MX6 as template (1). Screening was performed by fluorescence microscopy.

Strains expressing YFP-Ste4 were generated by integrating a plasmid containing the *STE4* promoter regulating the expression of *YFP-STE4* in a pRS406 backbone. Spontaneous loop-out events were selected by plating the cells on 5-FOA (5-fluoro-orotic-acid) plates.

To express a wild-type copy of *BUD4* in our W303-derived strain, we integrated a *BUD4*^{S288C}-pRS404 plasmid linearized with StuI. This plasmid contains only the C-terminal region of *BUD4* and, once integrated, results in a strain with only one functional copy of the gene. Conversely, to express the *bud4* mutant allele from W303 in S288C, *bud4*^{W303}-pRS405, also linearized by StuI digestion, was integrated. Due to gene conversion (7), it was necessary to screen more than 40 clones by analyzing the budding pattern.

A Cdc24-m1-expressing strain was made by integrating the plasmid *cdc24-m1-YFP*-pRS406, digested with XcmI, at the endogenous *CDC24* locus. Positive clones were selected based on the absence of nuclear localization (8).

Plasmids

Plasmids used in this work are listed in Table S3. Primers are included in Table S4.

For the cloning *BUD4* from W303 or S288C, a PCR fragment including the C-terminal and the 3'UTR (+2323 bp from the ATG to 152bp downstream of the stop codon) was generated using genomic DNA from ACL379 or BY4741 as template. The primers included on both ends 35-40 nucleotides homology arms to the pRS400 plasmid series. pRS404 was digested with NotI and Acc65I and the *BUD4* PCR fragment was cloned by isothermal assembly (9) to generate *BUD4*^{W303}-pRS404 and *BUD4*^{S288C}-pRS404. To change the *TRP1* marker to *LEU2*, *BUD4*^{S288C}-pRS404 and pRS405 were digested with BglI, and the corresponding fragments were purified and ligated to form *BUD4*^{W303}-pRS405. By sequencing the constructed plasmids, the *BUD4* mutation in W303 was confirmed: a deletion of one of the four Gs at +2456-2459 bp, counting from the ATG.

To generate plasmids carrying *cdc24-m1*, two overlapping PCR products were generated. The first one included a 20-nucleotide upstream homology arm to the pRS400 plasmid series and spanned from +119 to 581 bp of the *CDC24* ORF. The second PCR product started 522 bp after the ATG, continued until 201 bp after the stop codon, and ended with a 20-nucleotide homology arm. The S189F (+565) mutation was introduced in both internal primers. The resulting PCR products were cloned by isothermal assembly in NotI/Acc65I-digested pRS404. This plasmid was named *cdc24-m1*-pRS404. To

generate the YFP tagged version of Cdc24-m1, a BglII fragment from a plasmid containing *CDC24-YFP-*T_{ADH1} was ligated into the BglII site at +2235 of the *CDC24* ORF in *cdc24-m1*-pRS404.

Dose-response curves

Cells carrying pPRM1-YFP were grown in synthetic medium until mid-exponential phase. The cultures were then mildly sonicated, diluted to 6×10^5 cells/mL, and treated with different α-factor concentrations in 384-well glass-bottom plates (Brooks) for 2 h at 30°C. All media were supplemented with 0.1% w/v PEG (MW3550, Sigma) to block unspecific binding of pheromone to plastic material. Finally, cycloheximide was added to a final concentration of 100 μg/mL to inhibit translation, and the cultures were incubated at 30°C for at least 2 h more to allow complete maturation of YFP. Fluorescence microscopy-based cytometry was done as described elsewhere (11).

Polarization time dynamics and MP shape determination

The method was adapted from reference 3. Based on bright-field and maximum-projection time-lapse images of Bem1-3xmNG fluorescence, cells were segmented using CellID (11) and, based on cell boundaries, cell masks were generated using ImageJ. The mean (μ) and standard deviation (σ) of the intensity of mNG fluorescence from the pixels associated to each cell were then calculated at the different time points. The coefficient of variation (CV=σ/μ) was used to compensate for the difference in σ correlated to the total amount of Bem1 molecules (μ).

To analyze the shape of MPs, a circumference was manually fitted on each cell so that its curvature matched that of the MP using ImageJ. The radius of this circle was considered as the curvature radius of the projection.

Supplementary Tables

Table S1. Strains used in this study.

Strain	Genetic Background	Relevant genotype	Reference
ACL379	W303	*MATa Δbar1 can1::pHO-CAN1 ho::pOH-ADE2 leu2-3,112 trp1-1 can1-100 ura3-1 ade2-1 his3-11,15*	(2)
BY4741	S288C	*MATa his3Δ1 leu2Δ0 met15Δ0 ura3Δ0*	(12)
TCY3064	W303	*Δbar1 STE4::YFP-STE4*	*This work*
TCY3154	W303	*Δbar1 cdc28-as1 prm1::pPRM1-YFP-HIS3MX6 trp1::pACT1-CFP-TRP1-pRS404*	(2)
YRB3862	W303	*Δbar1 Δspa2::KANMX6 prm1::pPRM1-mCherry-HphMX4 STL1::pSTL1-CFP-TRP1*	(13)
YRP3865	W303	*Δbar1 Δpea2::KANMX6 prm1::pPRM1-mCherry-HphMX4 STL1::pSTL1-CFP-TRP1*	(13)
YGV5097	W303	*Δbar1 BEM1::BEM1-3xmNeonGreen-HIS3MX6*	(1)
YGV5259	W303	*Δbar1 Δrax1::HIS3MX6*	*This work*
YGV5405	W303	*Δbar1 Δrsr1::HIS3MX6*	*This work*
YGV5408	W303	*Δbar1 Δrax1::HIS3MX6 Δaxl2::TRP1*	*This work*
YGV5429	W303	*Δbar1 Δbud8::KANMX6*	*This work*
YGV5433	W303	*Δbar1 Δaxl2::TRP1 Δbud9::NATMX6 Δbud8::KANMX6*	*This work*
YGV5486	W303	*Δbar1 Δrsr1::HIS3MX6 BEM1::BEM1-3xmNeonGreen-KANMX6*	*This work*
YDV5654	S288C	*Δbar1::URA3*	(14)
YGV5655	S288C	*Δbar1::URA3 Δrsr1::KANMX6*	*This work*
YGV5765	W303	*Δbar1 bud4^{W303}::BUD4^{S288C}-TRP1-pRS404*	*This work*
YGV5831	S288C	*Δbar1::URA3 bud4::bud4^{W303}-LEU2-pRS405*	*This work*
YGV5836	W303	*Δbar1 Δspa2::KANMX6 prm1::pPRM1-mCherry-HphMX4 STL1::pSTL1-CFP-TRP1 BEM1::BEM1-3xmNeonGreen-HIS3MX6*	*This work*
YGV5838	W303	*Δbar1 Δrsr1::HIS3MX6 Δrax1::TRP1*	*This work*
YGV5839	W303	*Δbar1 Δaxl2::TRP1 Δbud9::NATMX6 Δbud8::KANMX6 Δrax1::HIS3MX6*	*This work*
YGV5879	W303	*Δbar1 Δrsr1::HIS3MX6 Δrax1::TRP1 BEM1::BEM1-3xmNeonGreen-KANMX6*	*This work*
YGV6017	W303	*Δbar1Δrga1::TRP1*	*This work*
YGV6035	W303	*Δbar1Δrga1::TRP1 Δrsr1::HIS3MX6 Δrax1::HphNT2*	*This work*
YGV6097	W303	*Δbar1 Δaxl2::HphNT1 Δbud9::NATMX6 Δbud8::KANMX6 CDC24::CDC24-YFP-TRP1-pRS404*	*This work*
YGV6100	W303	*Δbar1 Δaxl2::HphNT2 Δbud9::NATMX6 Δbud8::KANMX6 cdc24::cdc24-m1-YFP-TRP1-pRS404*	*This work*
YDV6164	S288C	*Δbar1::URA3 Δrsr1::KANMX6 Δrax1::HphNT2*	*This work*

Table S2. Summary of budding and default-MP-position phenotypes of mutant strains

Strain	MP default site		First bud position	Genetic background
	All low [αF] cells (G1 and cycling) and High [αF] G1 cells	High [αF] cycling cells		
Wild-type	Distal	Proximal	Distal & Proximal	W303
	Proximal		Proximal	S288C
BUD4^{S288C}	Proximal		Proximal	W303
bud4^{W303}	Distal		Distal & Proximal	S288C
Δaxl2	Distal		Distal	W303
Δbud8	Distal		Distal	W303
Δrsr1	Distal		Random	W303
	Distal		Random	S288C
Δaxl2 Δbud8 Δbud9	Distal		Distal	W303
Δrax1	Proximal		Proximal	W303
Δrax1 Δaxl2	Distal		Distal & Proximal	W303
Δrax1 Δaxl2 Δbud8 Δbud9	Distal		Random	W303
Δrsr1 Δrax1	Random		Random	W303
	Random		Random	S288C
Δrga1	Proximal		Proximal	W303
Δrga1 Δrsr1 Δrax1	Proximal		Proximal	W303

MP positioning in different deletion strains allowed determination of a hierarchy of landmarks. If the Bud4-Axl2 complex is intact, as in S288C-background strains, MPs follow this signal at the proximal pole, so as long Rsr1 is also active. In the absence of this strong cue, cells use the bipolar landmarks Bud8 or Bud9 for budding, as in W303-background strains. In both genetic backgrounds, we found that in response to pheromone, the distal Rax1-Rax2 activity can be independent of Bud8 or Bud9, as observed in *Δrsr1*, *Δbud8*, or *Δbud8 Δbud9 Δaxl2* strains. Rax1-Rax2 dominates in W303, where the use of Axl2 is weakened by the absence of Bud4. However, when the Rax1-Rax2 complex is inactivated in this background, the remaining Axl2 activity can drive polarization at the proximal pole, as can be deduced by comparing *Δrax1* and *Δrax1 Δaxl2* strain. This is similar to what happens during budding and what gave rise to the name of Rax1: Revert to AXial (5). Only when both budding cues and the Rax1-Rax2 complex are inactive (*Δrax1Δrsr1*), are random MPs observed in both the W303 and S288C backgrounds. The residual distal tendency observed in *Δbud8Δbud9Δaxl2Δrax1* compared to *Δrax1Δrsr1* suggests that Rsr1 has some distal positioning activity independent of protein landmarks. In summary, in decreasing order of strength, cues for MP positioning may be sorted as follows: $\mathbf{Axl2_{S288C}^{Proximal} > Rax1\text{-}Rax2^{Distal} > Axl2_{W303}^{Proximal} \geq Bud8^{Distal} > Rsr1^{Distal}}$

Table S3. List of plasmids used or constructed.

#	Name	Description	Reference
A1	pFA6a-KANMX6	P_{TEF} -kan^R-T_{TEF}	(6)
A2	pFA6a-TRP1	*TRP1*	(6)
A3	pFA6a-HIS3MX6	P_{TEF} -$HIS5^{S.\ pombe}$-T_{TEF}	(6)
A335	pFA6a-NATMX6	P_{TEF} -Nat^R-T_{TEF}	(15)
A666	pFA6a-HphNT2	P_{TEF} -$HygB^R$-T_{CYC1}	This work
A486	pFA6a-3xmNeonGreen-HIS3MX6	3xmNeonGreen-T_{ADH1}-P_{TEF} -$HIS5^{S.\ pombe}$-T_{TEF}	(1)
A609	$BUD4^{W303}$-*pRS404*	5'$BUD4^{W303}$ and 3'UTR	This work
A610	$BUD4^{S288C}$-*pRS404*	5'$BUD4^{S288C}$ and 3'UTR	This work
A664	*cdc24-m1*-YFP-pRS404	5'$cdc24^{S189F}$-YFP in pRS404	This work
A665	$BUD4^{W303}$-*pRS405*	5'$BUD4^{W303}$ in pRS405	This work

Table S4. DNA sequence of oligos used for cloning

Name	Oligo sequence
BUD4_pRS_Fw	gtgagcgcgcgtaatacgactcactatagggcgaattggGTACGCACCTAAGCGAACAAG
BUD4_pRS_Rv	taaagggaacaaaagctggagctccaccgcggtggcATTCGAAATGAATGGGGATCTGTG
5'Arm_cdc24-m1_Fw	ctcactatagggcgaattggGGACTCACTGTTCCATATATGCGC
cdc24-m1_S189F_Rv	ACTTTCAAATCGTCAAATGCTATTACCGG
cdc24-m1_S189F_Fw	CCGGTAATAGCATTTGACGATTTGAAAGT
3'Arm_cdc24-m1_Rv	tggagctccaccgcggtggcCGCACAACCTAAAATACGATTACTATCG

Lowercase bases denote homology sequences to target DNA for recombination.

References

1. A. C. Ventura *et al.*, Utilization of extracellular information before ligand-receptor binding reaches equilibrium expands and shifts the input dynamic range. *Proc. Natl. Acad. Sci. U.S.A.* **111**, E3860-E3869 (2014).

2. A. Colman-Lerner *et al.*, Regulated cell-to-cell variation in a cell-fate decision system. *Nature* **437**, 699-706 (2005).

3. N. T. Henderson *et al.*, Ratiometric GPCR signaling enables directional sensing in yeast. *PLos Biol.* **17**, e3000484 (2019).

4. J. M. Dyer *et al.*, Tracking shallow chemical gradients by actin-driven wandering of the polarization site. *Curr. Biol.* **23**, 32-41 (2013).

5. A. Fujita *et al.*, Rax1, a protein required for the establishment of the bipolar budding pattern in yeast. *Gene* **327**, 161-169 (2004).

6. M. S. Longtine *et al.*, Additional modules for versatile and economical PCR-based gene deletion and modification in *Saccharomyces cerevisiae*. *Yeast* **14**, 953-961 (1998).

7. R. Rothstein, Targeting, disruption, replacement, and allele rescue: integrative DNA transformation in yeast. *Methods Enzymol.* **194**, 281-301 (1991).

8. Y. Shimada, M. P. Gulli, M. Peter, Nuclear sequestration of the exchange factor Cdc24 by Far1 regulates cell polarity during yeast mating. *Nat. Cell Biol.* **2**, 117-124 (2000).

9. D. G. Gibson *et al.*, Enzymatic assembly of DNA molecules up to several hundred kilobases. *Nat. Methods* **6**, 343-345 (2009).

10. A. Bush *et al.*, Yeast GPCR signaling reflects the fraction of occupied receptors, not the number. *Mol. Sys. Biol.* **12**, 898 (2016).

11. A. Bush, A. Chernomoretz, R. Yu, A. Gordon, A. Colman-Lerner, Using Cell-ID 1.4 with R for microscope-based cytometry. *Curr. Protoc. Mol. Biol.* **100**, 14.18.11-14.18.26 (2012).

12. C. B. Brachmann *et al.*, Designer deletion strains derived from *Saccharomyces cerevisiae* S288C: A useful set of strains and plasmids for PCR-mediated gene disruption and other applications. *Yeast* **14**, 115-132 (1998).

13. R. Baltanás *et al.*, Pheromone-induced morphogenesis improves osmoadaptation capacity by activating the HOG MAPK pathway. *Sci. Signal.* **6**, 1-14 (2013).

14. C. G. Pesce *et al.*, Single-cell profiling screen identifies microtubule-dependent reduction of variability in signaling. *Mol. Sys. Biol.* **14**, e7390 (2018).

15. C. Janke *et al.*, A versatile toolbox for PCR-based tagging of yeast genes: New fluorescent proteins, more markers and promoter substitution cassettes. *Yeast* **21**, 947-962 (2004).